Advanced Steel Construction – Vol. 20 No. 2 (2024) 111–119
DOI:10.18057/IJASC.2024.20.2.2
(Special Issue: *11st International Conference on Advances in Steel Structures, ICASS'2023, Kuching, Sarawak, Malaysia*)

STUDY ON THE IMPACT CUSHIONING PERFORMANCE AND STRUCTURAL OPTIMIZATION OF A MODULAR COMPOSITE BUFFERING STRUCTURE

Yun-Tao Jin [1, 3] and Zhi-Xiang Yu [1, 2, 3, *]

[1] *School of Civil Engineering, Southwest Jiaotong University, Chengdu 610031, China*
[2] *National Engineering Laboratory for prevention and control of geological disasters in land transportation, Chengdu 611756, China*
[3] *Research Center of Protection Structures Against Natural Hazards, Southwest Jiaotong University, Chengdu 610031, China*
** (Corresponding author: E-mail: yzxzrq@swjtu.edu.cn)*

ABSTRACT

The traditional concrete rockfall shed, relying on a sand cushion for impact energy absorption, suffers from limited buffering performance, long recovery cycles, and inadequate resilience in emergency disaster prevention. To address these issues, this paper proposes a modular composite buffering structure comprising a flexible steel buffer and a sand cushion. A 500kJ impact test was conducted on the structure to investigate its mechanical behavior and rockfall cushioning performance. The test revealed the energy dissipation mechanism between the flexible steel buffer and the sand. Using the LS-DYNA platform, a FEM-DEM coupled dynamic numerical model was established to compare the cushioning performance of the buffering structure with other typical cushions. Additionally, the supports under the concrete slab and the structural layout of the flexible buffer were optimized to achieve better buffering and structural perfoemance. The research demonstrates that the composite buffering structure exhibits excellent cushioning performance, remaining intact under 500 kJ impact. Compared to sand material and EPS-sand cushion, the composite buffering structure reduces impact force by 62% and 20%, respectively. After replacing the supports under the slab by buckling corrugated tubes, the composite system is able to bear 1000kJ impact and the slab's bearing capacity is improved. With its superior cushioning performance, the composite buffering structure shows great potential for engineering applications.

ARTICLE HISTORY

Received: 8 April 2024
Revised: 13 May 2024
Accepted: 5 June 2024

KEYWORDS

Steel rockfall shed;
Rockfall impact;
Flexible steel structure;
Energy absorption;
Buckling corrugated tubes

1. Introduction

Approximately two-thirds of China's main land is mountainous area[1], posing a threat to human activities, especially the normal operation of transportation arteries, due to geological hazards such as landslides, debris flows and rockfalls. Rockfall disasters refer to the phenomenon of rocks rapidly rolling down from steep cliffs or slopes to the ground[2], and they are characterized by randomness and frequent occurrences[3]. When geological hazards such as rockfalls occur in mountainous areas, it is often not feasible to directly implement protective measures on the slopes adjacent to the transportation routes due to adverse geological conditions and the high risk of recurring rockfall disasters. Therefore, rockfall sheds[4-6], as they can be directly installed on roads, have become important protective measures for emergency response to geological disasters in mountainous areas. Traditional reinforced concrete rockfall sheds (Fig. 1a) have disadvantages such as long construction periods and low energy dissipation capacity. Additionally, the cushioning layer of rockfall sheds often utilize materials such as sand and gravels[7,8], resulting in limited buffering performance. These factors affect the impact resistance and emergency response capabilities of rockfall sheds. Therefore, the development of a steel rockfall shed structure with good buffering performance and fast assembly speed holds significant practical engineering significance and application value.

The rockfall shed is a common passive protective measure used for rockfall protection at tunnel entrances, exits, or sections prone to frequent rockfall disasters. Existing shed structures mainly consist of support structures and cushioning layers. The sheds achieve energy dissipation and impact diffusion of rockfall through the cushioning layer, reducing the impact force on the support structure, and ultimately intercepting the rockfall on the shed structure or guiding it to the specific area. Currently, steel sheds can be classified into two main types[9,10]: steel frame sheds and steel flexible sheds (Fig.1b, 1c). The steel flexible sheds combine arch-shaped steel structures with flexible protective nets. The flexible nets utilize their own deformation to intercept and cushion the rockfall, embodying the concept of "flexibility overcomes rigidity" in protection. Energy dissipation devices can also be installed when necessary[11,12], enhancing buffering and energy dissipation capabilities. In comparison, steel frame sheds have relatively higher stiffness and require the installation of a cushioning layer on the roof. Regarding shed supporting structures, Wang et al. conducted full-scale impact tests on a flexible steel shed[13], demonstrating that the flexible shed successfully intercepted rockfall under a 250kJ impact and only required simple maintenance for continued use. Tan proposed a flexible buffering structure based on the cable-supported structural principle and studied its deformation characteristics and energy dissipation capacity[14]. This cushioning structure can be flexibly applied to various shed structures. Wu et al. introduced a novel energy-dissipating and shock-absorbing shed by incorporating energy-dissipating supports[10], which increased the flexibility of the structure while maintaining its buffering capacity. Chen et al.[15] presented an optimized composite steel shed, in which the roof of the shed was optimized as a sandwich steel plate and the supports were optimized as thin-walled steel tubes to achieve secondary energy dissipation. They also developed a formula to calculate the internal forces of the optimized shed structure, and the results showed a reduction of approximately 20% in the maximum bending moment of the transverse and longitudinal beams after optimization. Yu et al.[16] proposed a new piston-rod-supported flexible structure system based on flexible protective nets. The system demonstrated buffering, self-recovery, and rock ejection capabilities, with an impact force approximately 60% of that of sand and EPS cushioning layers under the same impact energy. In terms of cushioning layers for sheds, the effect of a sand cushion on reinforced concrete slabs has been studied in literature[7]. The influence of parameters such as density, thickness of sand, and rock shape effect on the impact force has also been investigated [8,17,18], but these cushion materials have high self-weight. In recent years, research on using EPS materials as cushion has gained popularity[19,20], and they have been combined with sand, geotextiles, and steel structures to achieve satisfactory buffering effects with a lower self-weight. Some scholars have even creatively used materials such as waste tires and tennis balls as cushioning layers for rockfall impact response studies[21,22], but these studies are still in the preliminary exploration stage. The aforementioned studies provide valuable insights for the selection of shed structures and cushioning layers. However, the mentioned cushions either have issues with high self-weight and insufficient buffering capacity or have compatibility issues with steel sheds. Although the piston-rod-supported flexible structure is compatible with steel sheds, controlling its deformation is challenging, and there is a risk of excessive deformation or direct collision between the rockfall and the shed roof slab after the flexible net is penetrated [23].

Therefore, this paper proposes a buffering structure that combines the flexible steel structure and sand cushion to fully utilize the superior buffering and energy dissipation performance of flexible protective structures while avoiding the problem of direct collision between rockfall and shed roof slab caused by deformation variability. A 500kJ full-scale impact test was conducted to verify the effectiveness of this combined cushioning structure. Based on the LS-DYNA explicit dynamic simulation platform, FEM-DEM coupled numerical models were established for this buffering structure and other representative cushioning layers, and the buffering effect, structural stresses, and deformations of these cushions were quantitatively compared. Finally, the structural optimization of the system especially the supporting improvement under the slab were carried out to achieve better buffering performance. The research results provide a theoretical basis for the engineering design of this type of cushioning structure.

(a) Reinforced concrete rock-shed (b) Steel frame rock-shed (c) Fexible steel rock-shed

Fig. 1 Different types of rockfall sheds

2. The composite buffering structure

2.1. Structural principles

The main focus of this paper is the buffering structure on the upper part of the steel shed. This composite buffering structure consists of a flexible steel buffer and a sand cushion, as shown in Fig. 2a. The flexible steel buffer is primarily composed of flexible interception nets, steel wire ropes, energy dissipaters, and steel supports. The steel supports include vertical supports and inclined supports to ensure the geometric integrity of the structural system. The top of the steel supports is a sliding node, allowing the steel wire ropes passing through it to slide semi-freely and dissipate energy through frictions. These steel structural components can be assembled quickly, providing strong emergency response capabilities and disaster resilience. Fig. 2b shows the front view of the assembled buffering structure with the steel shed, with space provided for vehicles underneath the steel shed. The reason for adding a layer of sand on top of the concrete slab beneath the flexible steel buffer is that it is impossible to accurately predict the deformation of such nonlinear large deformation structures in practical engineering environments due to uncertain factors such as the shape, size, impact position, and impact angle of the rockfalls. Moreover, the bullet effect[23] may cause penetrations of the flexible net. These uncertain factors can result in direct rigid collisions between the falling rocks and the shed slabs, causing significant structural damage or even structural failure.

As shown in Fig.2b, the rockfall contacts with the flexible net firstly, and the net panel drives the movement of the steel wire ropes. When the tension in the steel wire ropes reaches a threshold (the activation force of the energy dissipater), it will trigger the stretching of the connected energy dissipater. This controls the development of internal forces in the components and dissipates the impact energy. The energy dissipation in this stage occurs through the plastic deformation of the net panel, the frictional sliding of structural components, and the stretching of the energy dissipater, with the latter being the main energy dissipation approach. When the falling rock continue to move downward, it may collide with the sand cushion. At this point, the sand cushion plays a role in spreading the pressure and dissipates some of the impact energy through the internal friction of the sand particles. Throughout the entire impact process, there are various complexities such as geometric, material, and contact nonlinearities, making the mechanical behavior highly intricate. The energy control equation for this process can be determined by Eq (1), which assumes a single rockfall impact and neglects the rolling friction of the falling rock within the flexible net.

$$\int_0^{h_{max}} F(h)dh = E_{k0} + mgh_{max} = E_{ed} + E_{sld} + E_n + E_s \tag{1}$$

Where $F(h)$ represents the vertical impact force of the falling rock, h represents the vertical impact displacement, h_{max} represents the maximum impact displacement, E_{k0} represents the kinetic energy of the falling rock when it contact the net, m represents the mass of the falling rock, and g represents the gravity acceleration, which is taken as 9.81 m/s^2. E_{ed}, E_{sld}, E_n and E_s represent the energy dissipated through stretching of the energy dissipater, friction of the structural components, deformation of the net, and friction of the sand, respectively.

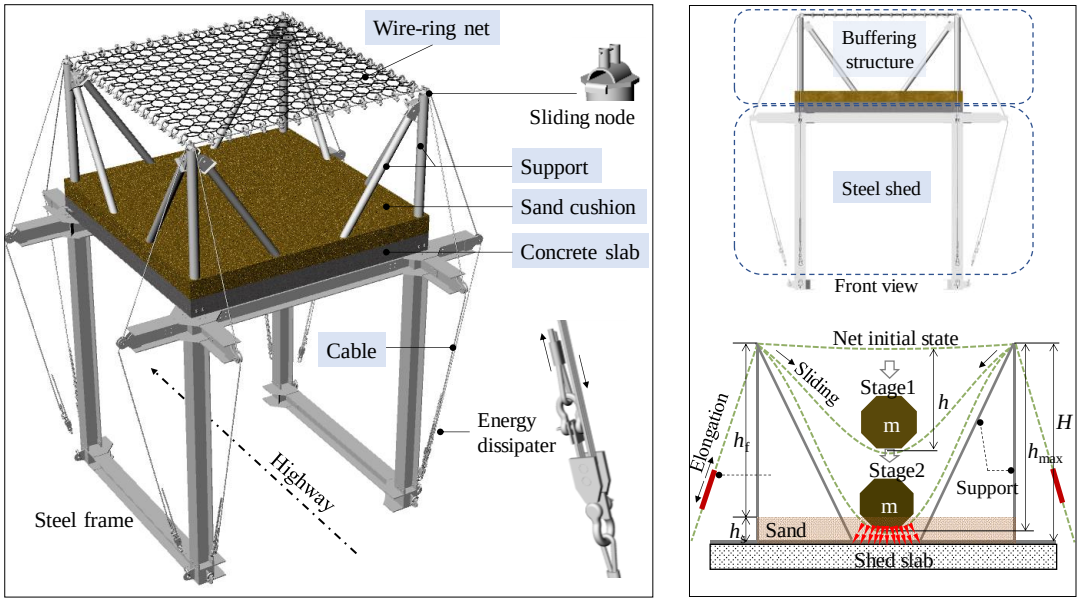

(a) Buffering structure fabricated with a steel rockfall shed (b) Front view and mechanism of the buffering structure

Fig. 2 The composition and working mechanism of the composite buffering structure

2.2. Test overview of the composite buffering structure

The full-scale impact test of the composite buffering structure was conducted at the National Engineering Laboratory for prevention and control of geological disasters in land transportation. The impact energy in the test was 500 kJ, and the test field is a comprehensive test platform with a testing capacity of up to 5000 kJ. The lifting and releasing of the impact block were achieved through a mobile crane with a maximum lifting height of 35 m (Fig. 3a). The

structural model of the test is shown in Fig.3b. It should be noted that in addition to the red triangle supports shown in the figure, there are also inclined supports, which are designed to meet the anchoring conditions of the end energy dissipaters at the test site to prevent excessive deformation caused by the extension cantilever. Otherwise it may affect the accuracy of the test results. The top of the steel support is designed to be slidable to facilitate the movement of the steel wire ropes (Fig. 3c), and the bottom of the vertical support is designed to be elastically rotatable (Fig. 3c). The impact block used in the test is a 26-faced polyhedron recommended in the European guidelines [25], with a mass of 6 tons (Fig. 3c). The bulk density of the sand cushion is 1480 kg/m^3. During the test, high-speed cameras were used to capture the impact images (Fig. 3c), and load cells were installed to measure the tension at the end of the steel wire ropes (Fig. 3c). The specifications of the components can be referred to Table 1, and other detailed test parameters can be found in the literature [24]. The test results will be compared and discussed with the numerical simulation results in Section 3.2.

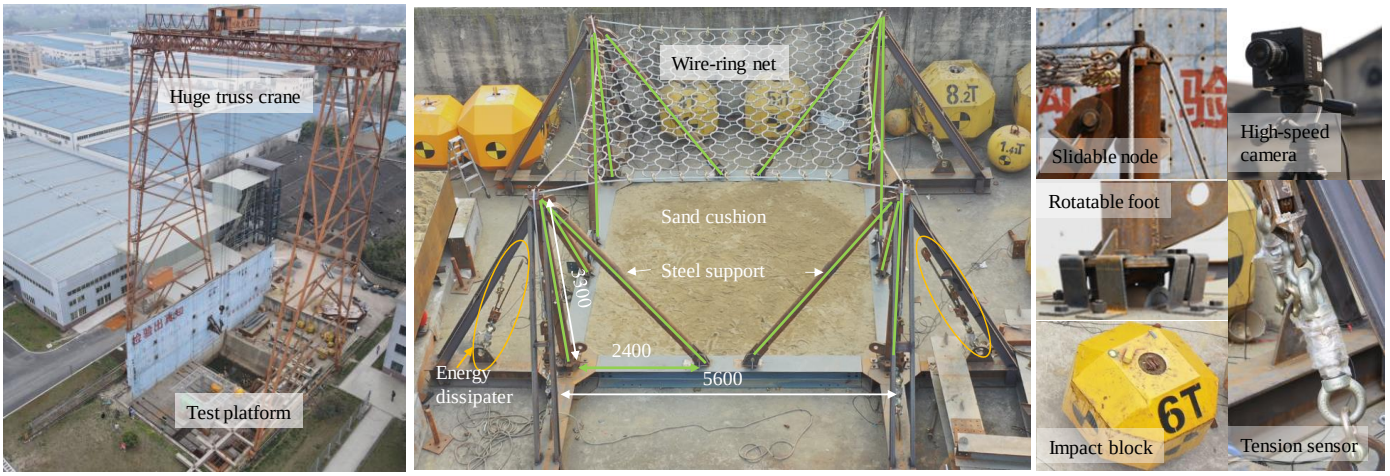

(a) Aerial view of the test field (b) Full-scale test structural model (c) Test equipments and nodes

Fig. 3 Layout of the experiment site

Table 1
Specifications of the members

Member	Specification	Material	Comment
Support	P180mm×8mm	Q235B	Tube
Wire-ring net	R19/3/300	Steel wire	1770 grade
Cable	Φ22mm	Steel wire	1770 grade
Energy dissipater	3@Φ16mm	Q235B	U-shaped
Sand	Medium sand	1480kg/m^3	4.3% water content

3. Numerical analysis of the composite buffering structure

3.1. Introduction of the numerical model

The numerical model in this study is based on the explicit dynamic analysis software LS-DYNA, utilizing the FEM - DEM coupling analysis method. This method allows for the simultaneous analysis of the dynamic responses of the falling rocks, flexible structures, sand cushion and reinforced concrete slab. The arrangement of the numerical model is shown in Fig. 4, and the dimensions of the concrete slab are 7000mm×6000mm×600mm. In the model, the falling rock and concrete slab are represented using solid elements, while the flexible net, supports, energy dissipaters, and steel rebars are represented using beam elements. The steel wire ropes are represented using cable elements, and the sand particles are represented using discrete elements with a radius of 15mm. In terms of material models, the falling rock is modeled as rigid bodies, the DEM particles are modeled as elastic materials, the flexible net and energy dissipaters are modeled using multi-linear elastoplastic material models, and the remaining steel components are modeled using ideal elastic-plastic material. The concrete is modeled using the CSCM Concrete material in LS-DYNA with a strength grade of 40 MPa. The specific parameter values are based on the literature [26]. Part of the input parameters for the materials are shown in Table 2, and the parameter values are based on the literature [27].

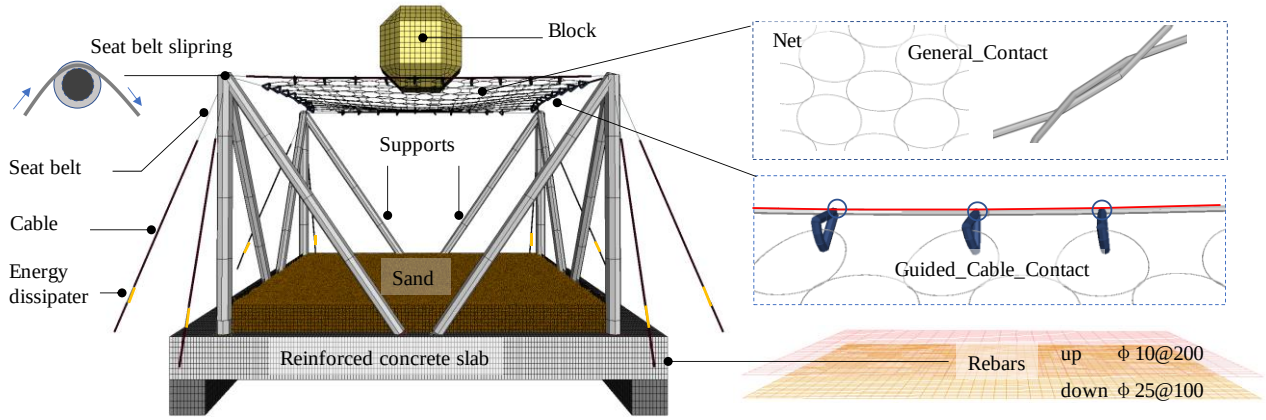

Fig. 4 Layout of the numerical mode

In this section, we specifically introduce two key steel structural components in the flexible buffer, the wire-ring net and the bar-shaped energy dissipater. As shown in Fig. 5a, the wire-ring net exhibits strong nonlinear characteristics under out-of-plane loading, with a tendency for the rings to transit from a curved shape to a straightened shape, accompanied by sliding between the rings. Influenced by geometric, material, and contact nonlinear factors, the force-displacement relationship during loading also shows a strong nonlinear correlation, which can be divided into stages dominated by flexural behavior and tensile behavior. Due to the considerations of geometric nesting relationships and actual contact conditions during modeling, the net in the model is able to reproduce the actual mechanical behaviors under impact. The energy dissipater plays a crucial role in the system by absorbing energy. As

shown in Fig. 5b, it typically remains in an elastic state before activation. When the tension in the steel wire rope exceeds the activation force, the energy dissipater starts to operate, leading to a significant energy dissipation. The bar-shaped energy dissipater used in this study is achieved by winding steel rebars around an axis pin and stretching it, utilizing its own plastic deformation and frictions between the steel bars and the axis pin for energy dissipation. In the computational model, a beam element with a special stress-strain relationship or a nonlinear elastic-plastic spring element consistent with the actual force-displacement relationship of the energy dissipater is employed to reproduce the behavior. This approach ensures efficient computation of the overall model while maintaining consistency with the mechanical behavior.

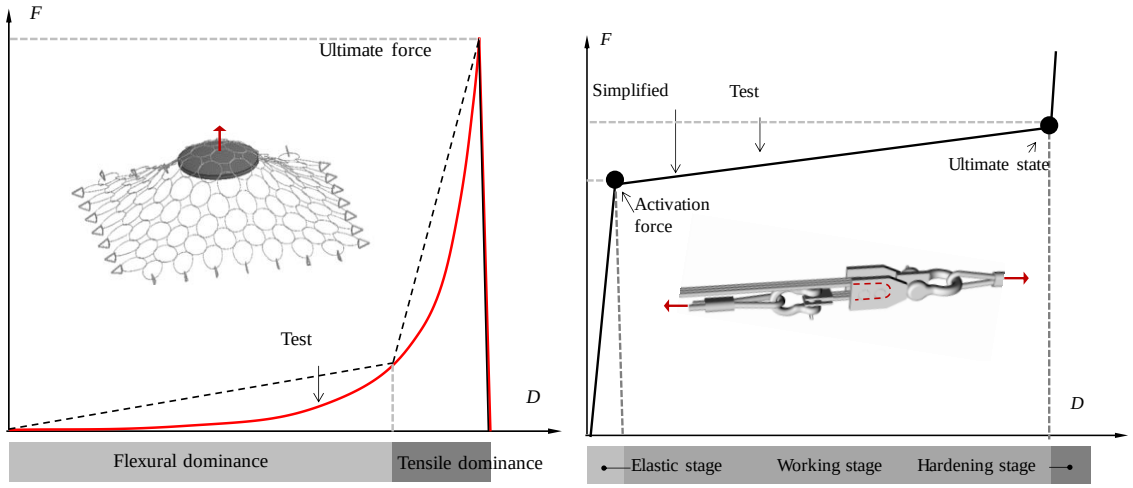

(a) Typical *F-D* curve of the wire-ring net

(b) Typical *F-D* curve of the energy dissipater

Fig. 5 Working characteristics of key components

Table 2
Parameters input of the materials

Member	Density	Elastic modulus	Poison's ratio	Yield stress	Failure strain
Wire-ring	7850kg/m^3	2.07×10^5 MPa	0.3	1488MPa	0.14
Energy dissipater	7850kg/m^3	2.06×10^5 MPa	0.25	1100MPa	1.61
Cable	7850kg/m^3	1.2×10^5 MPa	0.35	1770 MPa	0.015
Supports	7850kg/m^3	2.06×10^5 MPa	0.3	235 MPa	0.25
Block	2500kg/m^3	2.0×10^4 MPa	0.2	-	-
Bebar	7850kg/m^3	2.06×10^5 MPa	0.3	335 MPa	0.2
DEM	1480kg/m^3	2.1×10^4 MPa	0.25	-	-

3.2. Comparation analysis with the test responses

In the numerical model that is compared with the test results, all degrees of freedom of the nodes in the bottom concrete slab were fully constrained, so the boundary stiffness was consistent with the sand cushion in direct contact with the ground in the actual experiment. The images at the moment of maximum deformation for the experiment and simulation are shown in Fig. 6a and 6b, respectively. All structural components remained intact, and the deformation patterns of the flexible nets are consistent, with both coming into contact with the sand cushion. The steel supports did not undergo significant deformation, and the mesh shape of the flexible net underwent significant changes, with sliding deformation occurring along the steel wire ropes at the edge of the net. The sag of the steel wire ropes significantly increased compared to the state before the experiment, indicating that the energy dissipaters connected to the steel wire ropes underwent tension deformation. The displacement history comparison in Fig. 6c shows that the maximum displacements for the experiment and simulation are 3.493m and 3.381m, respectively. The simulated displacement is slightly smaller than the experimental value, with an error of less than 5%. One of the most important indicators for evaluating the bufferperformance of the cushion is the impact force or acceleration of falling rocks, and these two can be converted using Eq (2).

$$F = F_{fb} + F_{sl} = m(a+g) \tag{2}$$

Where F is the vertical impact force on the block. F_{fb}, F_{sl} is the vertical contact force of the flexible net and the sand on the block, and a is the acceleration of the block. The acceleration history curves of the block for the experiment and simulation are shown in Fig. 7a. The peak accelerations for the experiment and simulation are 122 m/s^2 and 133 m/s^2, respectively, with a relative error of 9%. When converted to impact forces, they are 791 kN and 857 kN, respectively. The time-history curve shows a steep peak in the impact force around t = 0.3 s, and the high-speed image during the experiment reveals that the moment of rapid increase in impact force occurs at t=0.29s, which is the instant of contact between the block and the sand cushion. The numerical simulation results indicate that at this moment, more than 90% of the energy of the falling block has already been dissipated, indicating that the energy dissipation of the sand cushion is relatively small but has a significant impact on the increase in impact force. Fig. 7b shows the comparison of the maximum tensions in the steel wire ropes between the experiment and simulation. Both the peak value and duration are consistent, and the tension is lower than the tensile strength of the 22mm-diameter steel wire rope utilizing high strength steel wires with a tension strength of 1770MPa. Fig. 7c presents the time-history results of the maximum axial force in the simulated circular beam elements. The peak tension is 24.5 kN, which is much lower than the tensile strength of the wire windings in the R19/3/300 wire-ring net[28-30].

The steel supports are made of low-carbon steel with a strength grade of 235 MPa. The stress distribution at the maximum load moment is shown in Fig. 8a, with a maximum stress of 99.4 MPa. The conservative approach was taken in selecting the cross-section values, and further optimization is considered in the following sections. The stress distribution nephogram of the wire-rings within the flexible net (Fig. 8b) indicates that the wire strands experience the maximum tension at the corners and the area in contact with the block. The main tension direction is at a 45-degree diagonal, which is different from the main tension direction in a flexible barrier [27]. This is because, in the given structural arrangement, the stiffness of the corner boundaries is slightly greater than that of the cables in the middle, which reflects the self-adaptive stiffness characteristics of the flexible structure.

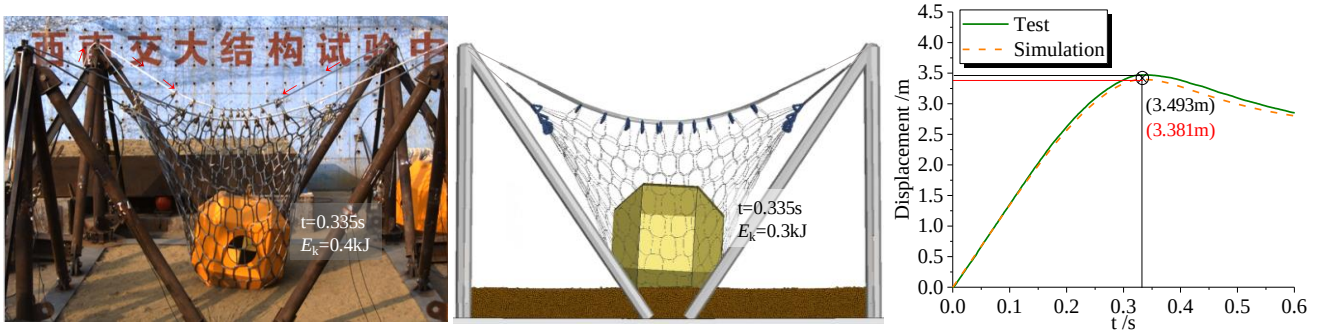

(a) The test image at maximum deformation moment (b) the simulation image at maximum deformation (c) block displacement history of the test and simulation

Fig. 6 Deformation comparation of the test and simulation result

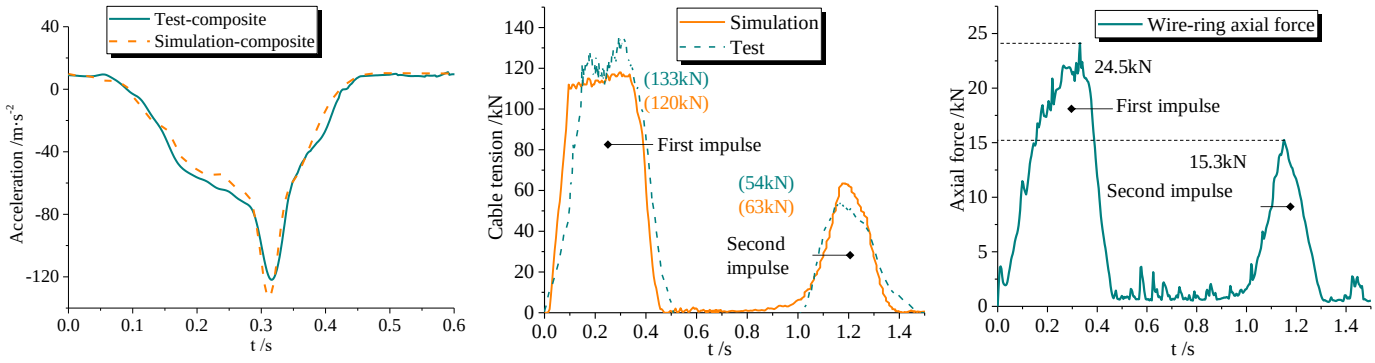

(a) The block acceleration history comparation (b) The cable tension comparison (c) The simulated wire-ring axial force history

Fig. 7 Impact responses of different parts

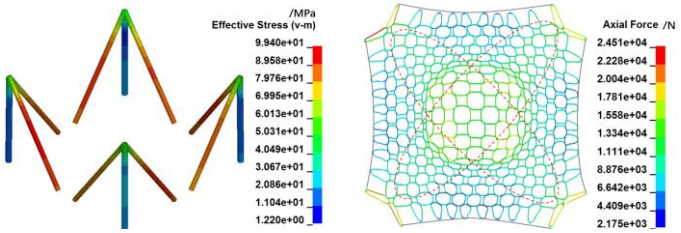

(a) Stress nephogram of the steel supports (b) Axial force nephogram of the ring net

Fig. 8 The stress state of steel components

3.3. Comparation analysis with typical cushions

In order to compare the buffering performance of the proposed composite buffering structure, numerical models of the rockfall impact on the sand cushion and EPS-sand composite cushion were also established based on the numerical approach described in Section 3.1, as shown in Fig. 9. The selected EPS material has a density of 30 kg/m^3 and a thickness of 2 m, with a sand layer thickness of 0.4 m on the top. In the model covering only with the sand cushion, the thickness of the sand cushion is 0.8 m. The EPS material model adopts a multi-linear elastoplastic material model, and specific input parameters can be referred to reference[20]. Other parameters in the model can be referred to in Section 3.1. In the three models, the impact energy when the rock bottom reaches the height of the net shown in Fig. 9c is 500 kJ. The simulation results (Fig. 10) show that among the three cushions, the proposed composite buffering structure has the smallest impact force, measuring 852 kN. The EPS-sand layer has the second smallest impact force, measuring 1055 kN. The traditional sand cushion has the largest impact force, measuring 2242 kN. The impact force of the flexible buffering structure is 62% lower than that of the traditional sand cushion and 20% lower than that of the EPS-sand cushion, indicating its superior buffering effect. In addition, from the time-history curve of the impact force in Fig.10, it shows that the flexible buffering structure also has the longest impact duration, which is beneficial for reducing the impact force according to the theorem of impulse.

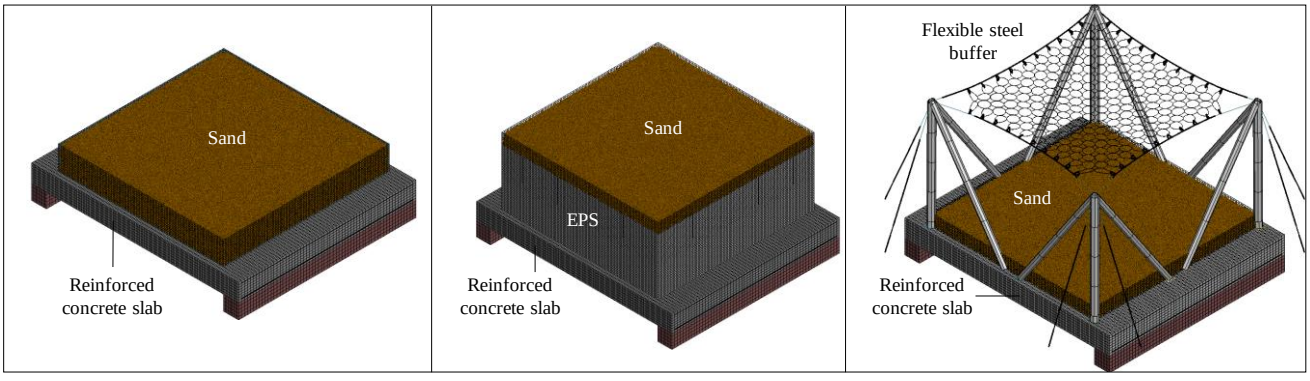

(a) 0.8m-thick sand cushion (b) 2m EPS-0.4m sand cushion (c) Composite buffering structure in this paper

Fig. 9 Three different rockfall cushions for responses comparation

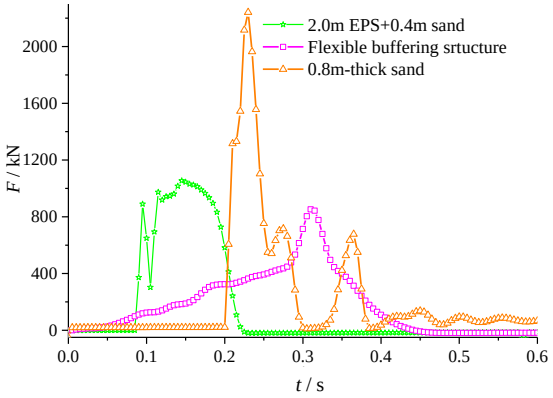

Fig. 10 Impact force history of the three different cushions

From the perspective of impact deformation, the composite buffering structure has the largest impact deformation, measuring 3382 mm (Fig.11c); the impact penetration depth of the sand cushion is the second largest, measuring 742 mm (Fig.11a); and the impact penetration depth of the EPS-sand composite cushion is the smallest, measuring 715 mm (Fig.11b). Interestingly, in combination with the results of the peak impact force mentioned above, the impact force of the EPS-sand composite cushion, which has a smaller impact deformation compared to the sand cushion, is actually smaller. This indicates that in the context of impact problems, it is not sufficient to simply compare the impact deformation to infer the relative magnitude of the impact force. The distribution of the impact force over time is also important and needs to be analyzed in conjunction with the actual situation. The distribution of compression stress in the bottom reinforced concrete slab is shown in Fig. 12. The concrete with a sand cushion has the highest compression stress, measuring 28.0 MPa. The concrete slab covered with the flexible buffering structure has the second highest stress, measuring 13.3 MPa. And the concrete slab covered with the EPS-sand composite cushion has the lowest stress, measuring 10.1 MPa. Although the impact force of the composite flexible buffering structure is the smallest according to the results in Fig. 10, the stress in the bottom concrete slab is higher than that in the EPS-sand composite cushion. This is because the arrangement of steel supports in the flexible buffering structure is not optimal. The inclined supports are located at the mid-span of the slab, resulting in a significant concentrated load at the mid-span, leading to local stress concentration and larger bending moments in the slab. This issue will be addressed and optimized in Section 3.4. The stress nephogram of the steel rebars in the concrete slab is shown in Fig. 12b. Similar to the stress state in the concrete, the maximum stress is observed in the scenario with a pure sand cushion, while the minimum stress is observed in the scenario with the EPS-sand composite cushion.

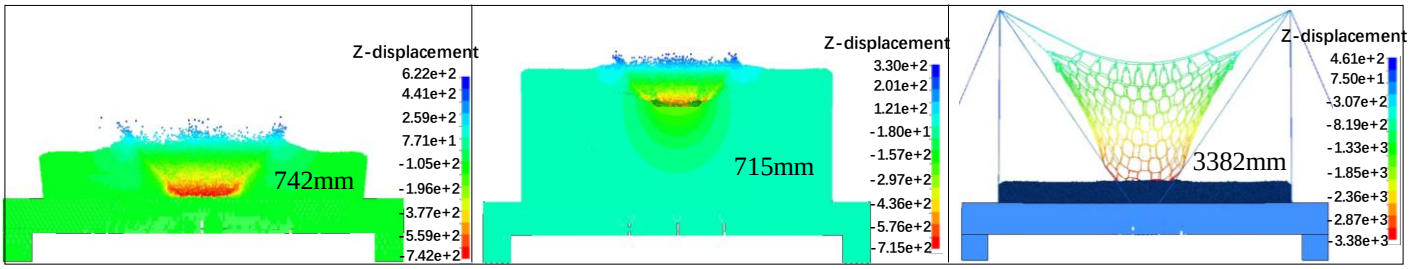

(a) 0.8m-thick sand cushion (b) 2m EPS-0.4m sand cushion (c) Composite buffering structure in this paper

Fig. 11 The maximum deformation nephogram of the cushions

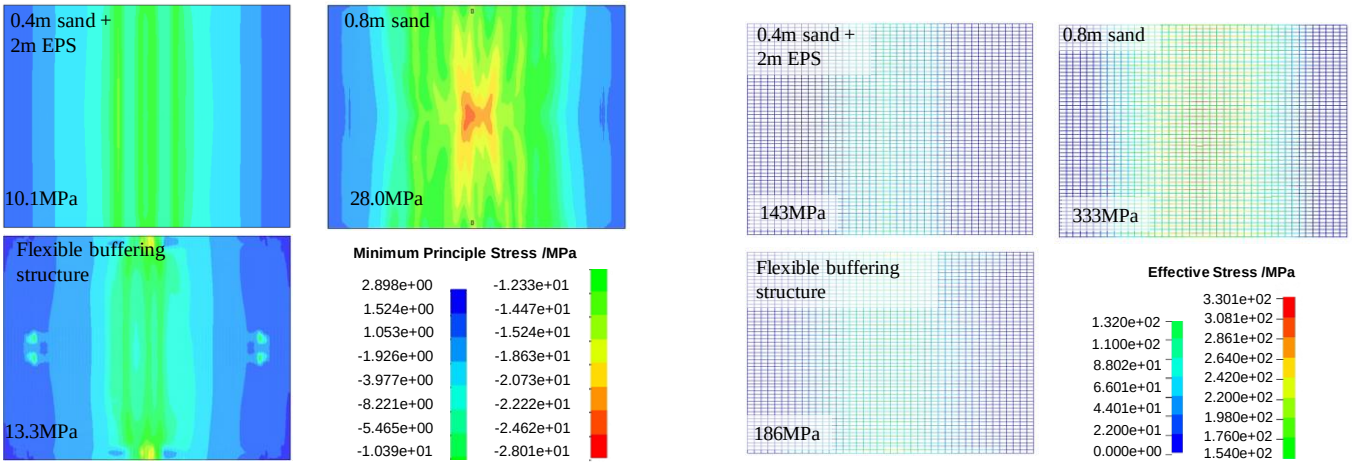

(a) Compression stress nephograms of the slabs (b) Von-Mises stress nephograms of the rebars

Fig. 12 Stress state of the reinforced concrete slab

4. Structural optimization

4.1. Optimization of the upper buffering structure

This section focuses on the layout optimization of the upper steel supports since the diagonal supports are located near the mid-span of the concrete slab and are subjected to significant compression, this results in large bending moments in the bottom slab. Therefore, an optimization of the steel supports is conducted. The specific optimization involves removing the inclined supports and using a horizontal support to connect the top of the vertical supports, along with diagonal connections using cables with diameter of 18mm. The numerical model was applied 500kJ impact with the same condition in Section 3.3. The maximum effective stress in the optimized steel supports is reduced to 89.5 MPa, which is a 10% reduction compared to the original structure (Fig.13a). More importantly, the compression stress in the concrete slab decreases to 8.05 MPa (Fig. 13b), with a reduction of 39.5%, and the stress in the bottom steel rebars decreases to 108.6 MPa (Fig. 13c), with a reduction of 41.6%. This optimization approach provides significant stress reduction for the protective object at the bottom, resolving the contradiction described in Section 3.3, where the composite buffering structure has low impact force but imposes a large load on the bottom slab. The maximum tension in the diagonal cables during impact is only 14kN，which means low internal forces in cables.

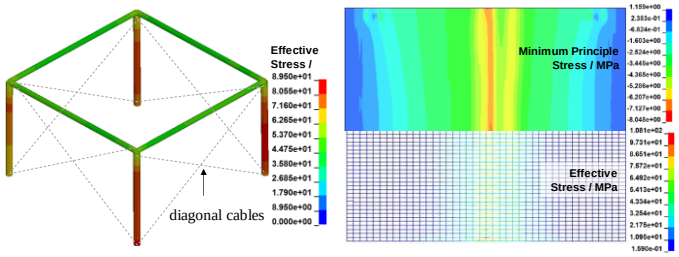

(a) Stress nephogram of the steel supports (b) Stress nephogram of the reinforced slab

Fig. 13 The stress nephogram of the structure after layout optimization

4.2. Buckling corrugated tubes for the slab supporting

To consider larger impact energy of the rockfalls, better adapt to the variability of rockfall hazards in actual field environments, and improve the impact resistance of concrete slabs under composite buffer structures during end-stage impact, a numerical analysis was conducted by replacing the supports of the slab with corrugated steel tubes. Previous studies have been carried out on similar tube supports [10,15], but the impact resistance of these corrugated tubes within the framework of this study still needs further research. The structure and dimensions of the corrugated steel tube used are shown in Fig. 14. The diameter of the corrugated tube D = 270mm, the height H = 300mm, the radius of the circular wave r = 25mm, the central angle corresponding to the arc is 60°, and the wall thickness of the metal tube t = 6mm. The material used is Q235B steel which is cost-effective in engineering application. End plates with a thickness of 10mm are welded at the upper and lower ends of the corrugated tube, and they are locked in by lock plates. The upper lock plate can be connected to a shear connector embedded into the concrete slab. The dimensions of the concrete slab in this analysis case are consistent with that in Section 3.3, with three corrugated tube supports on each side of the slab, totaling six supports.

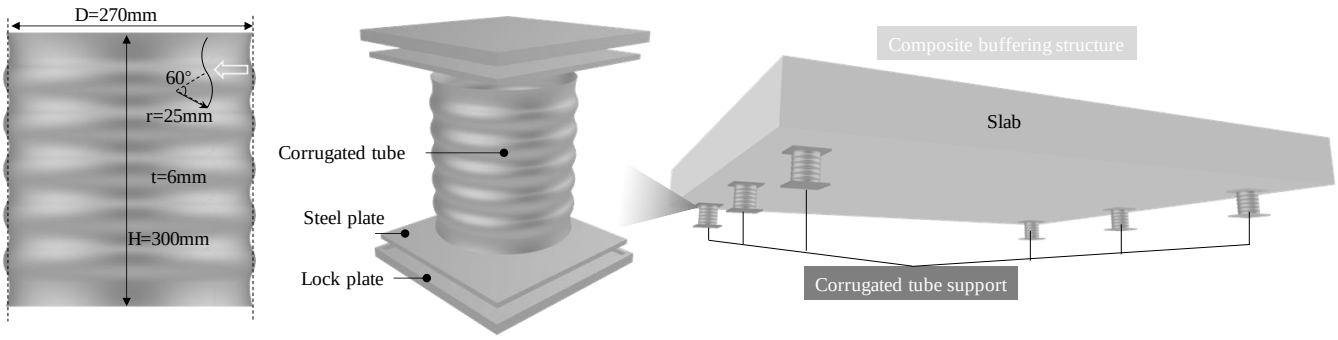

Fig. 14 Buckling corrugated tubes for supporting the shed slab

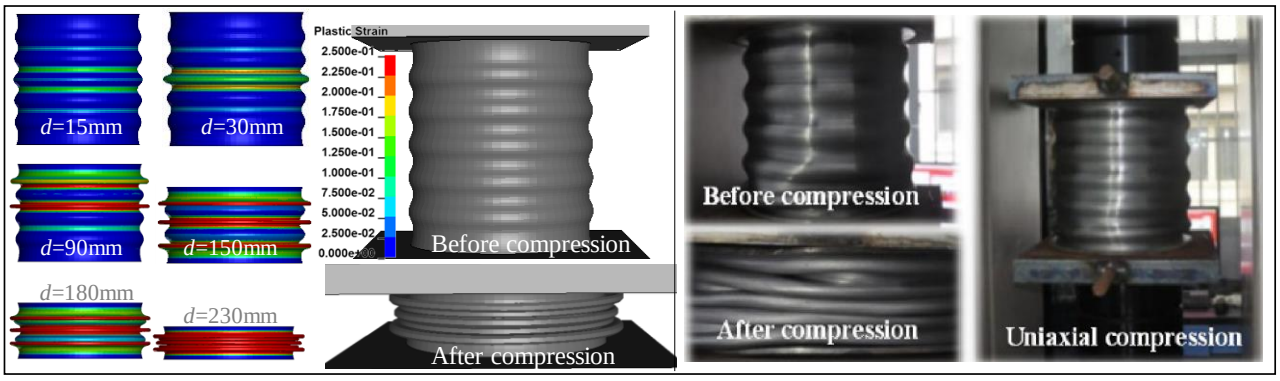

(a) Axial compression simulation of the corrugated tube (b) Axial compression test of the tube[10]

Fig. 15 Axial compression performance of the corrugated tube

Before using the corrugated tubes in the composite buffering structure and slab supporting, it is necessary to clarify its axial compression performance. Therefore, a uniaxial compression simulation of the corrugated tube was conducted, compared and verified against experimental results[10]. The compression test was modeled in LS-DYNA, with the steel tube established using shell elements. Self-contact was considered for thin-walled tubes to account for contact force transmission and stiffness evolution after bending deformation of the tube, as shown in Fig. 15a. The simulation results show significant plastic deformation occurring at the two grooves in the middle of the corrugated tube at a compression displacement of d = 15mm. At d = 30mm, plastic deformation also occurred at the convex wave between the two grooves, with further plastic deformation increases at the grooves. At d = 90mm, significant flattening occurred at the upper and middle circular areas of the tube, leading to self-contact of the tube-walls, with vertical loads being transmitted through squeezing between the tube-walls. During the compression process from d = 150mm to 230mm, more waves underwent large deformations and were flattened. The corresponding corrugated tube before and after compression in the experiment is shown in Fig. 15b, where the post-compression state aligns closely with the simulation results, forming dense compressed annular folds.

The compressive force-displacement curves of the corrugated tubes' compression process is shown in Fig. 16, where the simulated curve matches the experimental results, with buckling initiation force around 600 kN. Particularly, the simulation highly reproduced the undulations in the plateau segment of the curve, which is the stiffness evolution result of the process of corrugated tube-wall buckling, folding, and re-contacting, playing a crucial role in vertical force transmission. It shows that in the later stages of compression, the steel tube, due to the stacking of tube walls to form a contact-compression whole, exhibits a stiffening development, providing reliable support strength for the slab. The ultimate energy absorption of a single corrugated tube in simulation and experiment is 147 kJ and 134 kJ, respectively, with an error within 10%. The corrugated tube demonstrates superior buckling fuse function in static loading test and can consume considerable energy.

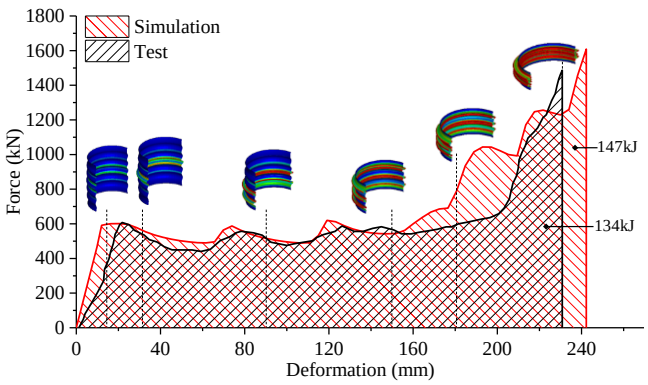

Fig. 16 F-D curves of axial compression of the corrugated tubes

After the corrugated tube was calibrated through static calculations, it was applied to the bottom supporting of the rock-shed slab under the protection of the composite buffering structure in this study to verify its buffering capacity for the slab under high kinetic energy impact exceeding the design level. The numerical model is essentially consistent with the composite buffering structure case in Section 3.3, with the only modification being the replacement of rigid supports with corrugated tube supports at the bottom of the concrete slab. A 1000 kJ rockfall impact simulation on the system was conducted, and the responses of the system under corrugated tube supporting are compared with that of rigid supporting at the same energy level. The established dynamic simulation model and its impact process are shown in Fig. 17, with the layout of the corrugated tubes in top view detailed in Fig. 17a, with a total of 6 corrugated tubes supporting on both sides. The gravity is gradually applied to 9.81 m/s^2 in the first 0.5 seconds of the calculation to achieve a stable state of system components and sand cushion under gravity, at which point the rockfall is just about to contact the flexible net. At t=0.70 s, the rock collided with the sand cushion and developed a significant impact force. At this moment, the bottom corrugated tubes are about to undergo significant buckling deformation, and the wire-ring net has experienced substantial sliding and deformation (Fig. 17b). At t=0.83 seconds, the rock has reached near the lowest point of the impact, and the supporting corrugated tubes have undergone significant buckling deformation (Fig. 17c), with compression deformations ranging from 59 mm to72 mm. The buckling deformation pattern is somewhat different from the fully symmetrical situation observed in static loading, possibly due to uneven vertical loading caused by the deflection of the concrete slab and certain horizontal shear forces acting on the tubes.

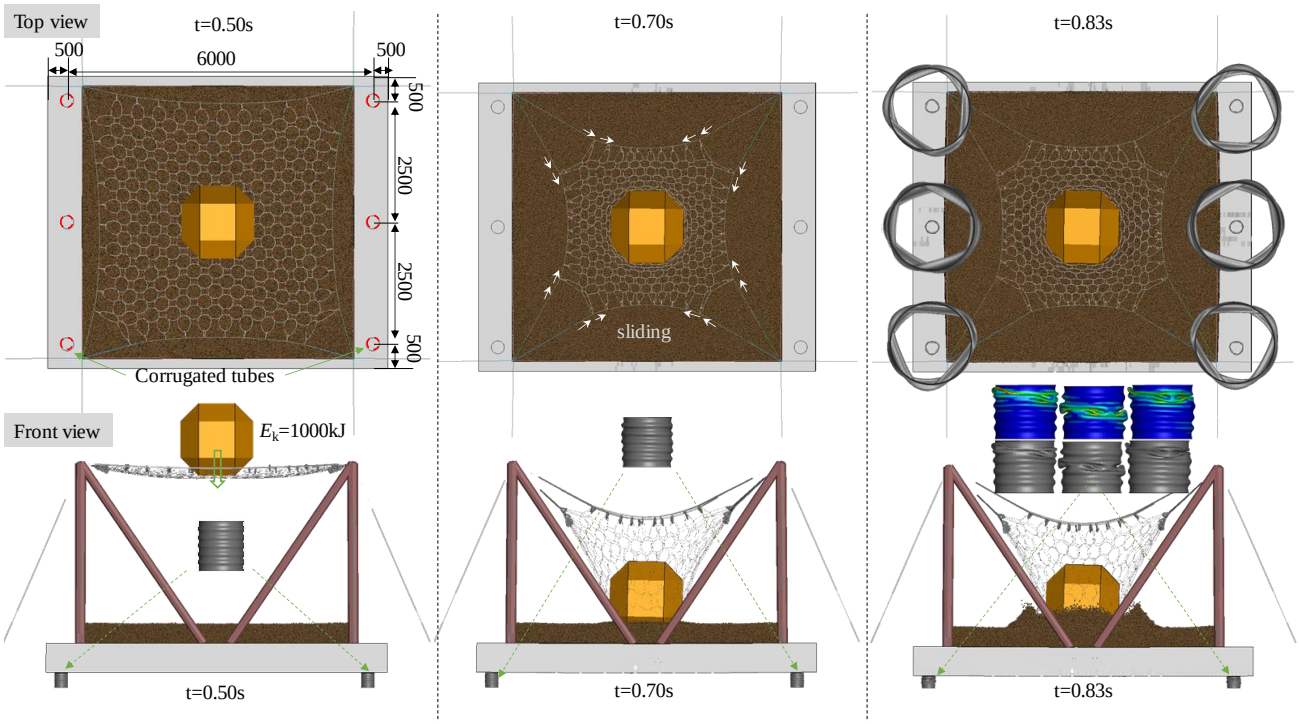

(a) t=0.50s initial state (b) t=0.70s impact state (c) t=0.83s impact state

Fig. 17 1000kJ impact process on the slab with the cushioning of composite buffering structure and the corrugated tubes supporting

Under the same 1000 kJ impact level, the impact responses of the composite buffering structure-slab with rigid supporting and corrugated tube supporting are compared as shown in Fig. 18. As observed in Fig. 18a, the maximum compressive stress of the concrete slab is reduced from 38.5 MPa under rigid supporting condition to 30.3 MPa, with a stress reduction of up to 21.3%, indicating a significant improvement. In Fig. 18b, the maximum impact reaction force can be reduced from 5351 kN under rigid supporting condition to 2505 kN, representing a reduction of 53.2%. The buffering effect is evident, and in the force-history curve under corrugated tube supporting condition, the plateau near the peak is more pronounced. This is a result of the combined action of the flexible buffering structure and corrugated tubes, with the corrugated tubes playing a key role in reducing the impact force peak when the rock collides the slab. Fig. 18b also presents the internal energy- history curve of the corrugated tubes, with a total energy absorption of 140 kJ under this calculation condition. The stress and deformation nephogram of the concrete slab under the two aforementioned supporting conditions are shown in Fig. 19. The maximum impact deflection decreases from 31.4 mm under rigid supporting to 20.6 mm, representing a reduction of 34.4%.

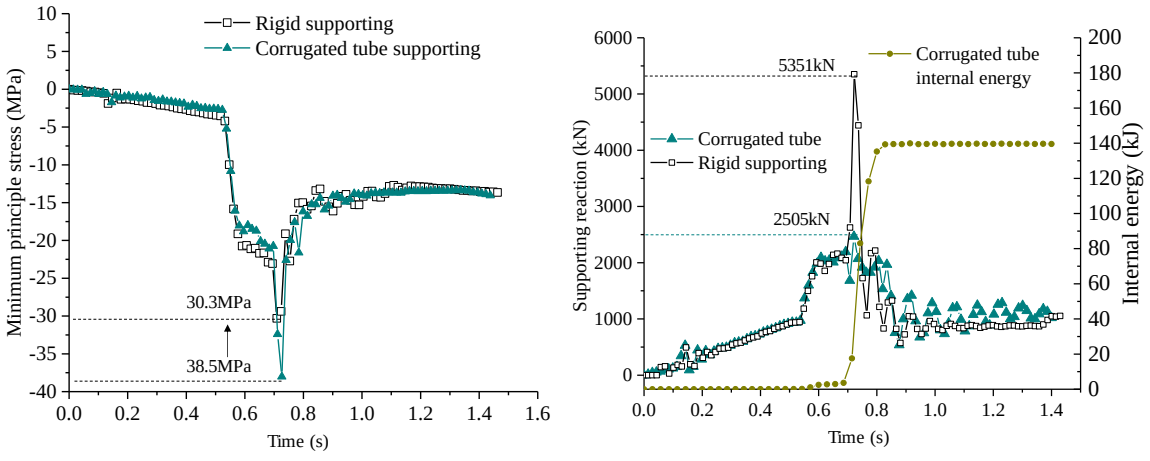

(a) Temporal maximum compression stress of slab (b) Temporal supporting reaction under the slab

Fig. 18 The concrete slab related responses using different supports

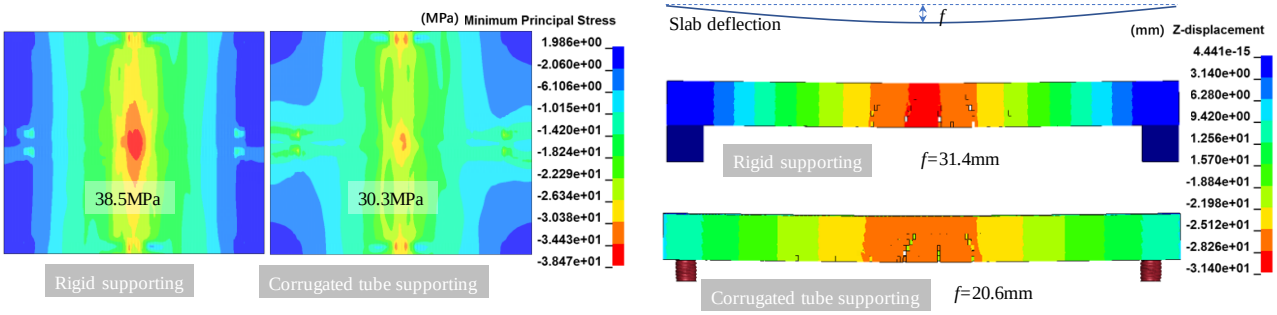

(a) Compression stress nephogram of slabs

(b) Maximum impact deflection of slabs

Fig. 19 The impact responses nephogram under the two supporting conditions

5. Conclusions

This paper proposes a composite buffering structure that combines a flexible steel buffer with a sand cushion. A full-scale 500 kJ impact test was conducted to validate the effectiveness of this type of structure. Based on the LS-DYNA explicit dynamic simulation platform, a coupled FEM-DEM numerical model was established for this buffering structure and currently typical cushioning layers. The buffering effects, structural stresses, and deformations of these cushions were quantitatively compared. Finally, structural optimizations especially the slab supporting optimization using corrugated tubes were performed, and the specific conclusions are as follows.

(1) The composite buffering structure is capable of withstanding impact energies of over 500 kJ while keeping the structure intact. The peak impact force in the experimental model was 787 kN, with the upper flexible steel buffer contributing significantly to energy dissipation and buffering, accounting for over 90% of the total energy dissipated. The sand cushion primarily serves as the second line of defense.

(2) The FEM-DEM coupled numerical model established based on the commercial code LS-DYNA effectively captures the dynamic behaviors of such structures, with errors in key responses such as impact force and displacement within 10%. Compared to the traditional sand cushion and the typical EPS-sand combination cushion, the proposed buffering structure in this paper can reduce the impact force by 62% and 20% respectively under a 500 kJ rockfall impact, demonstrating superior buffering performance.

(3) After upper structural optimization, the compression stress on the concrete slab and in the steel rebars can be reduced by 39.5% and 41.6%, respectively. When subjected to axial compression, corrugated steel tubes exhibit good buffering and energy absorption capabilities. When applied as supports for concrete slabs under the composite buffering structure, they can reduce the compressive stress on the slab by 21.3%, decrease the peak support reaction by 53.2%, and reduce the deflection of the slab by 34.4%. The proposed fast assembly composite buffering structure and the buckling corrugated-tube supports have high engineering application value.

Acknowledgements

This study is supported by the Key Research and Development Program of Sichuan Province (Grant No. 2022YFG0414), the Key Science and Technology Projects in the Transportation Industry in 2020 (Grant No. 2020-MS3-101).

References

[1] Yu Z.X., Zhao L., Liu Y.P., Zhao S.C. Xu H. and Chan S.L., Studies on flexible rockfall barriers for failure modes, mechanisms and design strategies: a case study of Western China, Landslides 16(2), 347-362, 2018.
[2] Volkwein A., Schellenberg K., Labiouse V., Agliardi F., Berger F., Bourrier, Dorren L.K.A., Gerber W. and Jaboyedoff M., Rockfall characterisation and structural protection –a review, Natural Hazards and Earth System Sciences, 11(9), 2617-2651, 2011.
[3] Luo G., Cheng Q., Shen W., Ling S., Zhang X., Zou P. and Zhao Y., Research Status and Development Trend of the High-Altitude Extremely-Energetic Rockfalls, Earth Science 47(3), 913-934, 2022.
[4] Kishi N., Konno H., Ikeda K. and Matsuoka K.G., Prototype impact tests on ultimate impact resistance of PC rock-sheds, International Journal of Impact Engineering, 27(9), 969-985, 2002.
[5] Delhomme F., Mommessin M., Mougin J.P. and Perrotin P., Behavior of a structurally dissipating rock-shed: experimental analysis and study of punching effects, International Journal of Solids and Structures, 42(14), 4204-4219, 2005.
[6] Mougin J.-P., Perrotin P., Mommessin M., Tonnelo J. and Agbossou A., Rock fall impact on reinforced concrete slab: an experimental approach, International Journal of Impact Engineering, 31(2), 169-183, 2005.
[7] Pichler B., Hellmich C. and Mang H.A., Impact of rocks onto gravel Design and evaluation of experiments, International Journal of Impact Engineering, 31(5), 559-578, 2005.
[8] Kawahara, S. Muro T., Effects of dry density and thickness of sandy soil on impact response due to rockfall, Journal of Terramechanics, 43(3), 329-340, 2006.
[9] Shi S.Q., Wang M., Peng X.Q., Yang Y.K., A new-type flexible rock-shed under the impact of rock block: initial experimental insights, Natural Hazards and Earth System Sciences, 13(12), 3329-3338, 2013.
[10] Wu Y., He S.M., Li X.P. and Wang D.P., Dynamic response and optimization of an inclined steel rock shed by the graded energy dissipating method, Journal of Mountain Science, 16(1), 138-152, 2019.
[11] Castanon-Jano L., Blanco-Fernandez E., Castro-Fresno D. and Ballester-Muñoz F., Energy Dissipating Devices in Falling Rock Protection Barriers, Rock Mechanics and Rock Engineering, 50(3), 603-619, 2016.
[12] Qi X., Xu H., Yu Z.X. and Zhao L., Meng Q.C., Dynamic mechanical property study of brake rings in flexible protective system, Engineering Mechanics, 35(09), 198-206, 2018.
[13] Wang M., Shi S., Cui L., Liu Y. and Yang Y., Experimental investigation on three-bay and single-span flexible rock-shed under impact of rockfall, China Civil Engineering Journal, 51(5), 1-11, 2018.
[14] Tan K., Flexible Multi-body Dynamics Simulation of Cable-supported structure for rockfall protection, Southwest Jiaotong University, 2018.
[15] Chen F., Chen H., Structure optimization and calculation method of combined shed-tunnel structure, The Chinese Journal of Geological Hazard and Control, 31(1), 1-10, 2020.
[16] Yu Z.X., Zhao L., Guo L.P., Liu Y.P., Yang C. and Zhao S.C., Full-Scale Impact Test and Numerical Simulation of a New-Type Resilient Rock-Shed Flexible Buffer Structure, Shock and Vibration, 1-16, 2019.
[17] Zhang Y., Xie L.Z., He B. and Zhao P., Research on the Impact Force of Rockfall Impacting Sand Cushions with Different Shapes. Applied Sciences, 122, 2022.
[18] Wang Y.S., Xu M., Yang C., Lu M.Y., Meng J., Wang Z.L. et al. Effects of elastoplastic strengthening of gravel soil on rockfall impact force and penetration depth. International Journal of Impact Engineering, 136, 2020.
[19] Ouyang C., Liu Y., Wang D. and He S., Dynamic Analysis of Rockfall Impacts on Geogrid Reinforced Soil and EPS Absorption Cushions, KSCE Journal of Civil Engineering, 23(1), 37-45, 2018.
[20] Ertugrul O.L., Kiwanuka A., Dynamic analysis of rock fall impact for a cantilever rock shed with geofoam cushion, European Journal of Environmental and Civil Engineering, 27(5), 1989-2014, 2022.
[21] Sun J., Chu Z., Liu Y., Luo W. and Wang M., Performance of Used Tire Cushion Layer under Rockfall Impact, Shock and Vibration, 1-10, 2016.
[22] Wang D.P. , Bi Y.Z. , Zhou L., Chen H., Zhou R. and Lovati M., Experimental study on physical model of waste tennis ball-sand composite shed cushion under rockfall impact, Bulletin of Engineering Geology and the Environment, 81(5), 2022.
[23] Mentani A., Giacomini A., Buzzi O., Govoni L., Gottardi G. and Fityus S., Numerical Modelling of a Low-Energy Rockfall Barrier: New Insight into the Bullet Effect, Rock Mechanics and Rock Engineering, 49(4), 1247-1262, 2015.
[24] Zou P., Design of Modular Steel Structural Flexible Shed and Research on its Anti-impact Performance, Southwest Jiaotong University, 2021.
[25] EOTA, Falling rock protection kits, European Assessment Document, 2018.
[26] Zhong H.Q., Yu Z.X., Zhang C., Lyu L. and Zhao L., Dynamic mechanical responses of reinforced concrete pier to debris avalanche impact based on the DEM-FEM coupled method, International Journal of Impact Engineering, 167, 104282, 2022.
[27] Xu H., Gentilini C., Yu Z.X., Qi X. and Zhao S.C., An energy allocation based design approach for flexible rockfall protection barriers, Engineering Structures, 173, 831-852, 2018.
[28] Yu Z.X., Liu C., Guo L.P., Zhao L. and Zhao S.C., Nonlinear Numerical Modeling of the Wire-Ring Net for Flexible Barriers, Shock and Vibration, 1-23, 2019.
[29] Jin Y.T., Yu Z.X., Guo L.P., Luo L.R., Zhang L.J. and Liao L.X., Tensile-bending stiffness coordinated model for wire-ring nets in flexible rockfall protection system, Chinese Journal of Rock Mechanics and Engineering, 42(3), 698-707, 2022.
[30] Liu C., Theory and method of discrete analysis for flexible protective structure against geological hazard on shallow Slope, Southwest Jiaotong University, 2020.